Inferring Polluted Asian Absorbing Aerosol Properties Using Decadal Scale AERONET Measurements and a MIE Model

SHUO WANG[1], Xinying Wang[2], and Jason Blake Cohen[3]

[1]Sun Yat-Sen University, School of Atmospheric Sciences
[2]School of Atmospheric Sciences
[3]School of Atmospheric Sciences, Sun Yat-Sen University

November 24, 2022

Abstract

Absorbing aerosols uniquely impact radiative forcing, aerosol chemical transport, and meteorology. This paper uniquely quantifies BC core and sulfate shell size and mass using decadal measurements of multi-spectral AOD, SSA, and AE from AERONET stations located throughout East, Southeast, and South Asia, in connection with a MIE model. All sites are uniquely characterized into four types: urban, biomass burning, long-range transport, and clean. The size and mass of the core and shell are calculated as probability distributions, and found to be unique within each classification. Well known urban, biomass burning, and clean sites are all properly identified. Furthermore, two unique sites previously thought to not have multiple characteristics are identified, with urban and biomass burning significant in Beijing and long-range transport significant in the otherwise clean South China Sea at Taiping island. It is hoped that these results will allow for advances in attribution and radiative forcing studies.

Inferring Polluted Asian Absorbing Aerosol Properties Using Decadal Scale AERONET Measurements and a MIE Model

Shuo Wang[1], Xinying Wang[1], Jason Cohen[1,2*]

[1]School of Atmospheric Sciences, Sun Yat-Sen University, Guangzhou, China

[2]School of Environment Science and Spatial Informatics, China University of Mining and Technology, Xuzhou, China

Correspondence to: Jason Blake Cohen (jasonbc@alum.mit.edu)

Key Points:

- Aerosols are categorized into biomass burning, urban, and long-range types over Asia using decadal long multi-spectral measurements.
- Based on multiple AERONET SSA measurements and a MIE model, physical characteristics of different aerosol types are deduced.
- Most aerosols are found to be mixed, with two sites having different characteristics during different times of the year.

Abstract

Absorbing aerosols uniquely impact radiative forcing, aerosol chemical transport, and meteorology. This paper uniquely quantifies BC core and sulfate shell size and mass using decadal measurements of multi-spectral AOD, SSA, and AE from AERONET stations located throughout East, Southeast, and South Asia, in connection with a MIE model. All sites are uniquely characterized into four types: urban, biomass burning, long-range transport, and clean. The size and mass of the core and shell are calculated as probability distributions, and found to be unique within each classification. Well known urban, biomass burning, and clean sites are all properly identified. Furthermore, two unique sites previously thought to not have multiple characteristics are identified, with urban and biomass burning significant in Beijing and long-range transport significant in the otherwise clean South China Sea at Taiping island. It is hoped that these results will allow for advances in attribution and radiative forcing studies.

Plain Language Summary

Black Carbon (BC) strongly absorbs visible radiation, leading to unique impacts on atmospheric radiation, climate, the water cycle, and $PM_{2.5}$. This work attributes different aerosol source characteristics, and further specifies the size distribution and concentration of aerosol BC cores and refractive shells. This work uses measurements of aerosol extinction (AOD), aerosol absorption fraction (SSA), and the wavelength-dependent difference in AOD (AE), in combination with statistics and a MIE model (physical model of aerosol/radiation interaction) using a Core-shell approximation. The results show that aerosols observed in East, Southeast, and South Asia can be uniquely classified into four types: urban, biomass burning, long-range transport, and clean. These results are consistent in terms of aerosol size and mass at each site within each type of characterization. Furthermore, 2 unique sites are identified in which a second characteristic occurs some significant fraction of every year, which otherwise was not known or previously identified in the literature. These results are expected to help enhance the understanding of attribution of aerosols, as well as provide specific size and mass details of the aerosols useful to improve radiative forcing models and aerosol impacts on climate change.

1 Introduction

Aerosol has been identified as one of the largest contributors to the uncertainty in our understanding of a diverse set of environmental issues including: the earth's radiation balance and climate change [*Chung and Seinfeld*, 2005; *Jacobson*, 2001; *Ramanathan and Carmichael*, 2008], surface loadings of air pollution [*Ichoku et al.*, 2008; *Langmann et al.*, 2009; *Rosenfeld*, 1999; *Sinyuk et al.*, 2007], and acid rain [*Charlson and Wigley*, 1994; *Stockwell et al.*, 1990; *C Wang*, 2013; *Zhang et al.*, 2004], among others. Furthermore, aerosols indirectly impact the lifetime, size, phase, and other properties of clouds, which in turn further impact the Earth's radiative balance and precipitation [*Rosenfeld et al.*, 2014; *Tao et al.*, 2012]. The major sources of aerosols come from combustion of fossil fuels [*Parry et al.*, 2007; *Reuter et al.*, 2014; *Tang et al.*, 2013] and biomass burning [*Cohen et al.*, 2011; *D Kim et al.*, 2008; *Ming et al.*, 2010], with significant changes in aerosols associated with changes in economics, population, energy consumption, and other social systems. Changes in aerosols occur in terms of magnitude as well as spatial-temporal variation, especially as different regions undergo different pathways of development [*Cohen et al.*, 2017; *C Lin et al.*, 2020a; *C Lin et al.*, 2020b; *S Wang et al.*, 2020a].

Quantitative properties of aerosol particles in-situ (including the concentration, size, chemical composition and optical properties) allow for a quantitative relationship to be made between aerosols, the environment and climate change [*Cohen*, 2014; *Cohen and Wang*, 2014; *Fast et al.*, 2006; *R Kahn et al.*, 1998; *C-Y Lin et al.*, 2014]. Some of the largest uncertainties have to do with connecting aerosols and the radiation balance, which itself is dependent on the optical properties, size, and mixing state of aerosols in the atmosphere [*Cai et al.*, 2020; *Cohen et al.*, 2011; *S Wang et al.*, 2020a]. The mixing state of aerosol particles impacts upon the amount of direct and scattered upward and downward radiative streams, atmosphere-radiative equilibrium, condensation of secondary species, cloud condensation and ice nuclei, water uptake, particle acidity, and aerosol chemistry [*Bondy et al.*, 2018; *Chew et al.*, 2013; *Schutgens and Stier*, 2014; *Zaveri et al.*, 2008]. Therefore, it is important to identify the source (urban, biomass burning, long-range transport), size (nucleation, fine, coarse, etc.) and mixing state of existing aerosol particles in order to accurately assess their direct and indirect effects on the atmosphere.

Accurate simulation of the aerosol mixing state and in-situ composition is an open question currently being addressed by the scientific community [*Andreae and Gelencsér*, 2006; *Kahnert et al.*, 2013; *Yuan et al.*, 2016]. One such approach is to represent aerosol particles as a set of concentric spherical Core-Shell layers (where the core consists of BC, and the shell consists of sulfate and/or nitrate). This system is both physically reasonable, and can be made to represent scattering and absorbing properties ranging those measured in the real world. In specific, it has been determined that a Core-Shell model usually produces a better match with aerosol properties observed in heavily polluted region, such as found in East, Southeast, and South Asia, where BC once discharged into the atmosphere is coated with sulfate or nitrogen oxides in a very short time [*Cohen and Wang*, 2014; *Peng et al.*, 2016; *Zhang et al.*, 2016]. Most current chemical transport models (CTMs), general circulation models (GCMs) and reanalysis products (such as WRF-Chem, GEOS-Chem, CESM-3, MERRA, NCEP, etc.) assume a non-Core-Shell approximation [*Ichoku and Ellison*, 2014; *P S Kim et al.*, 2015; *Matsui et al.*, 2013; *Nordmann et al.*, 2014; *Yu et al.*, 2012], meaning that while CTMs can resolve the atmospheric composition of unmixed aerosols reasonably well, there are intrinsic problems in terms of being able to predict the composition of aerosols under polluted conditions or which have undergone long-range transport, and further tend to underestimate their overall absorption of radiation [*Barsanti et al.*, 2013; *Cohen et al.*, 2011; *Kajino et al.*, 2012; *Lane et al.*, 2008]. The use of the Core-Shell model in this work is intended to aid elucidating how changes in measured atmospheric absorption and overall radiative properties of aerosols of different sizes and mixing ratios, can provide more insight into the sources and in-situ processing of observed BC.

The aerosol measurements used are measured from the AERONET network from 1997 through the present, using a Core-Shell approximation approach [*Oleg Dubovik et al.*, 2002]. A detailed analysis of the decadal AERONET optical measurements reveals important changes in the loadings, size and chemical composition of aerosols throughout most areas in East, South and Southeast Asia, due to rapid economic development, increasing urbanization, and increased population, among other factors. First, the measurements form AERONET are used to set different thresholds to make different classification with respect to the Aerosol

Optical Depth (AOD), Angstrom Exponent (AE), and Single Scatter Albedo (SSA). Second, using variance maximization and statistical fitting, the source type(s) of the measured aerosols are classified following the approach of [*C Lin et al.*, 2020a]. Third, a MIE model and statistical-analytical techniques are employed to constrain the size, and mixing state properties of the aerosols with radiation of different wavelengths in the visible and near infrared (VIS/NIR) to calculate the theoretical SSA. Finally, the modeled SSA is constrained by measurements of SSA consistently across all wavelengths, allowing a solution space to be derived that probabilistically describes the mixing state and particle size distribution consistent with the observations.

Our goal is to find an objective, clear, and simple way to systematically analyze the regional characteristics of aerosols, their sources, and in-situ environmental evolution. By connecting this approach with ground observations at known idealized urban, biomass burning, long-range transport, and other sites, a probabilistic set of source conditions can be quantified. This is then applied to other such sites around the world, allowing the contributions to the measured absorption to be better understood. This may lead to better controls on the loadings of particulate matter, especially so when different techniques for source control or impact mitigation should be made at the same geographic location under different atmospheric, climatological, and other environmental conditions. The results can further aid in understanding the contributions to human health, air quality, and the climate system, since the new relationship helps provide information both to the local user, as well as other users upwind or downwind.

2 Methods and Data

2.1 AERONET Measurements

Daily measurements of AOD at 440nm, 675nm, 870nm, and 1020nm were obtained from all AERONET stations in East Asia, South Asia, and Southeast Asia, using Level 2 direct solar products [*Holben et al.*, 1998] from March 1997 to May 2017. as a measure of the amount of absorbing aerosol, Level 2 inversion products corresponding to SSA at 440nm, 675nm, 870nm, and 1020nm were also obtained when AOD>0.4 [*Cohen and Wang*, 2014; *O Dubovik et al.*, 2000]. Angstrom

Exponent (AE) was computed based on AOD measurements at 440nm and 675nm, and particles with an AE<0.3 were removed due to possible cloud contamination.

2.2 Filtering and Grouping Highly Polluted Regions

To ensure all sites have a sufficient amount of AERONET inversion data so as to group the findings using variance maximization (following the method of [*C Lin et al.*, 2020a]), each site must have either 100 or more days of data with one of the three following conditions: high mean AOD (average AOD > 0.4), high extreme event AOD (one day of AOD > 1.0), highly variable AOD (standard deviation of AOD > 0.2), or more than 300 days of total measurements. This combination ensures that regions which have occasional extreme events such as biomass burning or long-range transport, are also considered alongside those regions which are more constantly polluted, such as urban areas. After filtering 67 sites remain for further analysis.

Determination coefficients (R^2, P > 95%) between all combinations of AOD, AE, and SSA (at 440nm), absolute mean values of AOD (at 440nm), the ratio of standard deviation of AOD to AOD (at 440nm), and the 90^{th} percentile and the 50^{th} percentile of the ratio of standard deviation of AOD to AOD (at 440nm) are used to categorize the 67 sites into four orthogonal groupings. The biomass burning group has increasingly smaller particle sizes as AOD increases (AE and AOD increase simultaneously), as well as a mean AOD greater than 0.5. Clean sites have a lower mean AOD (less than 0.5) and a lower absolute standard deviation ratio of AOD (less than 0.3). Urban sites have larger and less absorbing particles as AOD increases or larger particles as AOD increases, due to rapid deposition of secondary nitrate, sulfate, and low vapor pressure VOCs. This should be coupled with a not too large difference in extremes, here defined as the ratio between the 90^{th} percentile and the 50^{th} percentile of the probability density function (PDF) of the standard deviation ratio (ratio less than 2.65). Finally, long-range transport has more absorbing aerosols as AOD increases or larger particle size as AOD increases, due to high amounts of small absorbing aerosols emitted from the fires, which slowly age and oxidize as they are transported far downwind; combined with a very high standard deviation (the ratio of the 90^{th} to 50^{th} percentile of the standard deviation of AOD to AOD ratio is more than 2.65), as consistent with the growth of aerosol particles in-situ for an extended period [*Cohen and Wang*, 2014; *Cohen et al.*, 2011], as well as statistics of measurements

downwind from fires an observed by [*Cohen et al.*, 2017; *Deng et al.*, 2020; *C Lin et al.*, 2020b; *S Wang et al.*, 2020a].

2.3 Radiative Properties

A MIE model is applied to compute the radiative properties of hundreds of different combinations of sizes of Core-Shell mixed aerosols, using a BC core and a sulfate or nitrate shell of varying thicknesses following [*Haywood and Shine*, 1995]. In this work, the thickness of the BC core R_{core} and shell R_{shell} are varied in steps of 10nm each from 0.05μm to 0.50μm and 0.01μm to 0.80μm respectively, using best estimates of the respective real part [a] (2.0 for BC and 1.426 for sulfate) and imaginary part [b]*i (1.0 for BC and 0.0 for sulfate) [*D Kim et al.*, 2008; *Schuster et al.*, 2005]. This range of sizes allows for the full range of the fine mode fraction to be explored [*R A Kahn et al.*, 2010; *Van Donkelaar et al.*, 2016; *Weagle et al.*, 2018]. The resulting computed values of extinction efficiency (Q_{ext}) and absorption efficiency (Q_{abs}) are used to compute the SSA [*Zhang et al.*, 2008].

2.4 Model and Measurement Inter-comparison

A new metric is computed to constrain the modeled SSA uses simultaneous measurements across all four of the wavelength-dependent measurements from AERONET. First, the central 80% of the PDF of measured SSA is computed independently at each wavelength. Second, the union between these four sets is computed, herein called the Merged SSA (MSSA), as detailed in Equation 1.

$$MSSA = \left(\int_{0.1}^{0.9} SSA_{440}\right) \cap \left(\int_{0.1}^{0.9} SSA_{675}\right) \cap \left(\int_{0.1}^{0.9} SSA_{870}\right) \cap \left(\int_{0.1}^{0.9} SSA_{1020}\right) \quad \textbf{Equation 1}$$

The MSSA is subsequently used to constrain the modeled SSA as a function of core and shell size. The resulting set of R_{core} and R_{shell} form a solution space spanning at most a few hundred combinations. This space is hereby analyzed with two additional indices: The Aerosol Size Ratio (ASR) and the Aerosol Mass Ratio (AMR), which are respectively computed by equations 2a and 2b, and represent the individual size and mass ratios over the MSSA solution space.

$$ASR = \frac{R_{shell}}{R_{core}} = \frac{R_{total} - R_{core}}{R_{core}} \quad \textbf{Equation 2(a)}$$

$$AMR = \frac{M_{shell}}{M_{core}} = \frac{\rho_{shell} * (R_{total}^3 - R_{core}^3)}{\rho_{core} * R_{core}^3} \quad \textbf{Equation 2(b)}$$

Some sites classified as urban have a significant minority of days that also contain characteristics of biomass burning or long-range transport. To address this complexity, we separate extremely polluted days point-by-point and re-analyze the separated dataset. The extremes are separated by first computing the mean and the standard deviation of the AOD at 440nm and second separating all data greater than the mean plus one standard deviation. This procedure is repeated three times, merging each iteration of extremes with the previous extremes. This method has been shown to work well for extremes of OMI NO_2 and MISR AOD measurements [*Deng et al.*, 2020].

3 Results

The new method results in all stations being uniquely sorted into four groups: 13 biomass burning, 25 clean, 14 urban, and 15 long-range transport. In addition, we find 2 sites obviously are a mixture of more than one characteristic group occurring on a minority of days, and the other group occurring overall.

3.1 Grouping and Classification

The sites belonging to the biomass burning classification are given in Figure 1a, and are shown to have an AOD time series with most of the year being relatively clean and a short but intense period which is extremely polluted, with the difference ranging from a factor of 2.3 to 5.7. At each individual site these peaks occur annually with a similar magnitude, start time and end time every year. However, these magnitudes, start times and end times vary greatly between different sites. In addition, at all biomass burning sites, the correlation coefficient between the AOD and AE is always positive, with a maximum correlation coefficient of 0.43, consistent with a smaller particle size at higher pollution loadings which then undergo in-situ condensational growth.

Chiang Mai has the most overall data among these biomass burning sites (Figure 1b), and every year the extreme events occur exclusively from February to April. Furthermore, the mean AOD value is 0.73, and correlation coefficient between the AOD and AE is 0.18. It is also well known as a typical biomass burning site [*Cohen et al.*, 2017; *C Lin et al.*, 2020a]. For these reasons, Chiang Mai is used in the remainder of this study as the representative biomass burning site.

Unlike biomass burning regions, the clean regions do not have any obvious or recurring annual peak, have both an overall low absolute AOD value and variance. Among the sites in the clean group, Bandung is the most representative (Figure 1c). This side has the vast majority of its AOD lower than 0.5, and the ratio of variance of AOD to AOD is also concentrated around and below 0.5.

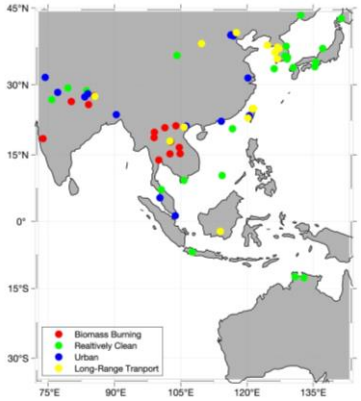

(a)

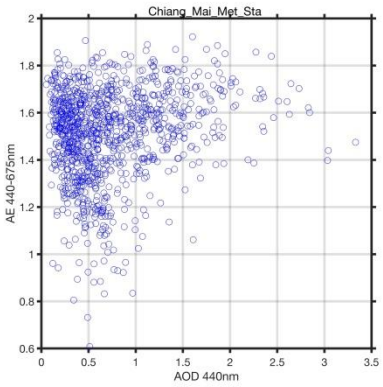

(b)

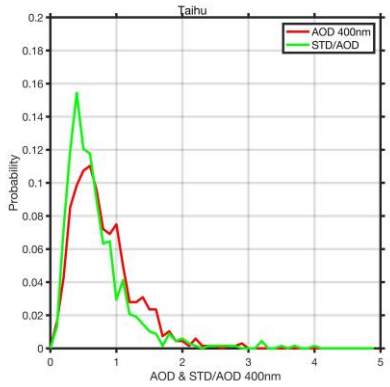

(c)

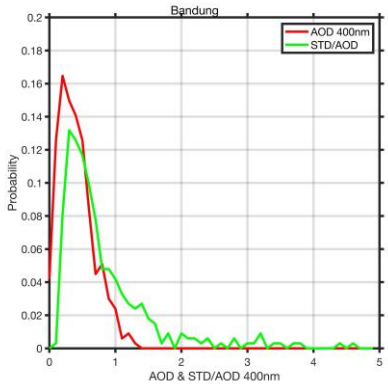

(d)

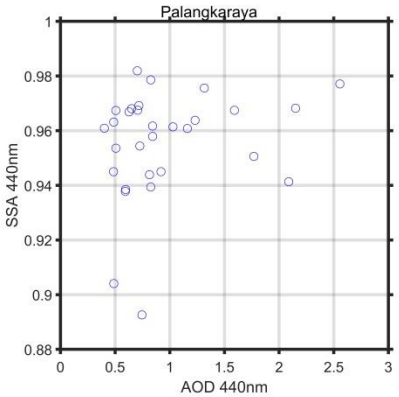

(e)

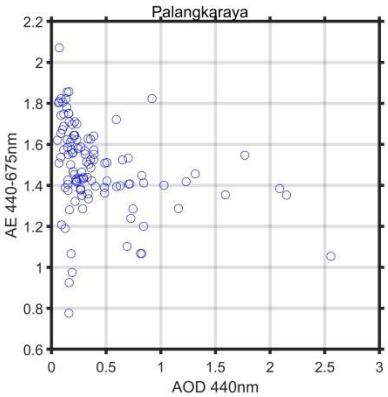

(f)

Figure 1. (a) distribution of all four different site types; (b) Chiang Mai; (c) Taihu; (d) Bandung; (e-f) Palangkaraya.

Urban regions have emissions that tend to be "quasi steady-state" over space and time, and hence the AOD time series is expected to have a relatively higher mean and lower variability when compared with other classifications [*Cohen and Prinn*, 2011], with the major source of variance being associated with local meteorology. The results show that the sites classified as urban have an increasing SSA with AOD, found to have a maximum and average of correlation of 0.48 and 0.34 respectively. In addition, they have a decreasing AE with increasing AOD, with a correlation ranging from -0.46 to -0.06. These results are consistent with pollution events enhanced by atmospheric stagnation, high concentration oxidant conditions leading to more coating of existing particles, and higher sulfate and nitrate formation, leading to an overall larger particle size and more scattering radiative profile. The statistically most representative urban site is Taihu (Figure 1d), which will subsequently be used as the representative urban site.

Those sites classified as long-range transport, when compared with urban sites have an average and standard deviation of AOD which is both higher and less stable (0.52 for AOD, and a factor of 3.3 for the 90^{th} percentile of the STD of AOD to AOD ratio). These results are consistent with an initial BC emission source that include no subsequent source of BC, while all secondary growth all occurs via expansion of the shell slowly in-situ. In this case, more radiation from the sun is reflected by the larger shell, while the thick shell reduces overall lensing, leading to less efficient secondary absorption by the BC core. The most representative site with this classification is Palangkaraya (central Indonesia, Figure 1e-f), with an AOD value of 0.41, a standard deviation of 0.44, and a very negative correlation coefficient of -0.32 between AOD and AE. The time series of decreasing AE does not occur randomly, but instead occurs only during certain times of the year that the wind is coming from the westward direction. The time series of AOD at Palangkaraya has some peaks that are much higher than the normal range of mean plus variability, with these special peaks only occurring in some years. When they occur, they always occur from late Winter through Spring time, and when they occur, they vary strongly in magnitude from event to event.

This explanation is consistent with highly aged black carbon from far away biomass burning sources know to occur in Sumatra or Borneo [*Cohen*, 2014] or elsewhere in Southeast Asia [*S Wang et al.*, 2020b] being transported into the city after undergoing significant aging, but are still significantly more absorbing than the local sources. The same phenomenon also occurs in other long-range transport regions, including Taiwan and Northeast China, South Korea, and Nepal.

3.2 Aerosol Physical Properties

The results of the measurement-constrained modeled SSA at Chiang Mai is given in Figure 2a. The solution space of the particle sizes is relatively thin (32.3 nm core size, 80 nm shell size) and the slope is relatively small. It is worth noting that first, there are almost no solutions available when the core size and shell size are greater than 220nm and 600 nm respectively, and second the total absorption of the particles is pretty high (SSA>0.83). In specific at smaller particle sizes, the SSA of the net aerosol particles is found to gradually increase, although the median and maximum are found to respectively be 0.90 and 0.93.

The ASR of Chiang Mai is found to have a median of 2.85, and a range from 2.25 to 4. Assuming that the actual density of BC has an uncertainty range from 1.8g/cm^3 to 2.3 g/cm^3 [*Cohen and Wang*, 2014], the corresponding AMR minimum ranges from 4.52 to 5.77, while the corresponding maximum ranges from 27.4 to 35. The solution spaces for core size, shell size, the ASR and the AMR are found to be uniform across all biomass burning sites.

The results of the measurement-constrained modeled SSA at Taihu is given in Figure 2b. The solution space of the particles is relatively broad (50.5 nm core size, 131.7 nm shell size) and the slope is relatively larger than Chiang Mai. It is noteworthy to see that the absorption of the particles is moderate (SSA>0.86). In specific at smaller particle sizes, the SSA of the particles is found to gradually increase, although the median and maximum are found to respectively be 0.92 and 0.95.

The ASR of Taihu is found to have quite a wide range, with a median of 3.64, and a range from 2.80 to 4.75. The corresponding AMR is also broader with a range from 9.11 to 59.0. Not all sites classified as urban have as similar an ASR and AMR as the sites classified as biomass burning. This is mainly due to the fact that while some

sources of urban aerosol particulates are continuous (i.e., power plants), others may vary (i.e., transportation and household burning), while the meteorology and photochemistry are both also more variable during the emissions times.

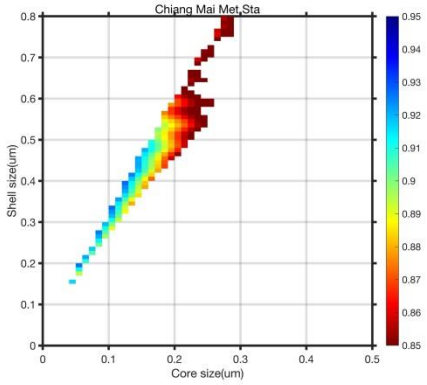

(a)

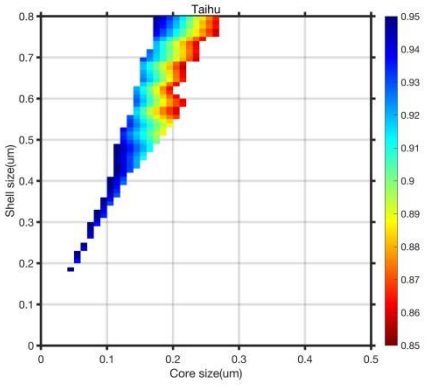

(b)

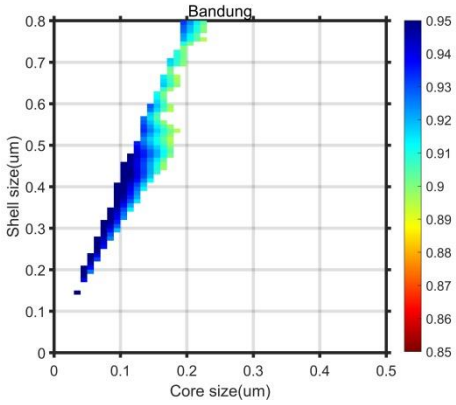

(c)

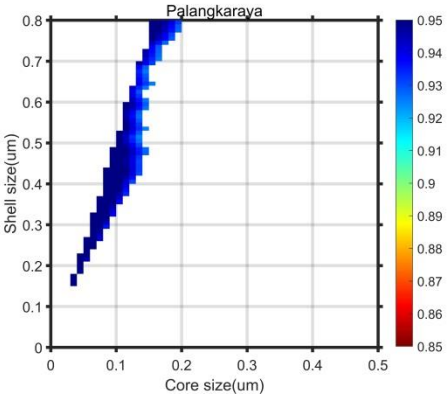

(d)

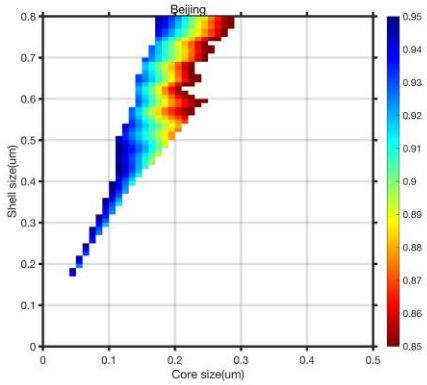

(e)

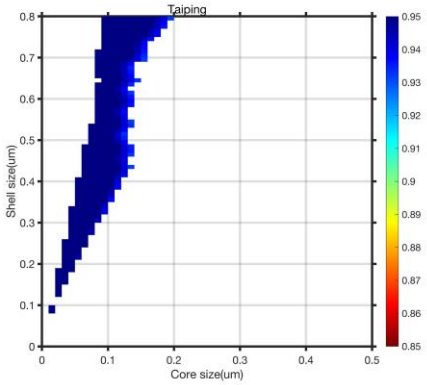

(f)

Figure 2. a MIE model results constrained by 4 wavelength AERONET SSA measurements. (a) Chiang Mai; (b) Taihu; (c) Bandung; (d) Palangkaraya; (e)Beijing; (f) Taiping.

The results of the measurement-constrained modeled SSA at Bandung is given in Figure 2c. The solution space of the particles is relatively broad in terms of both core and shell, and the slope is relatively less useful to interpret the results than in Taihu. It is noteworthy to see that the absorption of the particles is low (SSA>0.90). Overall, this site has a lower AOD, and a slightly wider range of ASR (from 2.81-5.25) and AMR (9.24-79.84).

The results of the measurement-constrained modeled SSA at Palangkaraya is given in Figure 2d. This site has the highest SSA value (>0.92), AMR (3.31-6.00) and ASR (15.30-120.) among the sites in this group. These results are consistent with long-range transport, wherein the aerosols were in the air longest and underwent the most amount of physical and chemical processing. The timing of the peaks in AOD is also consistent with the timing of the burning season in western Indonesia as well as super-long range transported burning from northern Southeast Asia. Similarly, the timing of the peaks in AOD at another long-range transport site (Chen Kung university) are found to occur at the same time as fire sources in Eastern India, Myanmar, and Northern Thailand, and therefore provides a second consistent story [*C Lin et al.*, 2020b; *S Wang et al.*, 2020a]. Other sites identified as long-range transport sites are found in South Korea and Northeast China.

PDFs of the core size, shell size and total particle size of each site are given in (Figure 3a-3d, 3g-3h). For BC, the proportion larger than 200nm in Chiang Mai (43%), which is much higher than elsewhere. Taihu has the second largest percent of BC larger than 200nm (26%). The remaining sites have 7% or less BC larger than 200nm (Figure 3g). These results are consistent with biomass burning and urban sources, where larger particles of BC tend to be produced. In terms of the shell size, Chiang Mai, Bandung and Palangkaraya all have a significant proportion of sulfate less than 400nm, ranging 22%, 26% and 27% respectively (Figure 3h), consistent with the source regions not having a large amount of nitrate or sulfate to condense. In Taihu, the proportion of sulfate less than 400nm is only 9%, while the proportion between 600nm and 800nm is

the largest at 63%, which is consistent with large amounts of locally emitted and secondarily produced nitrate and sulfate.

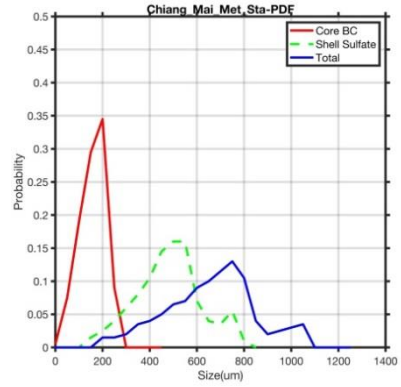

(a)

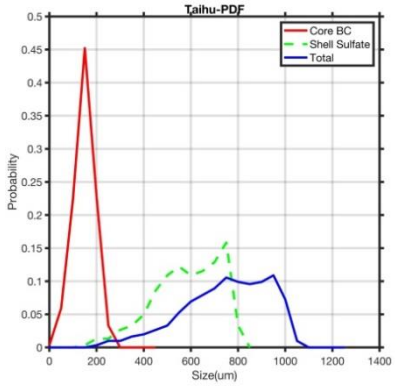

(b)

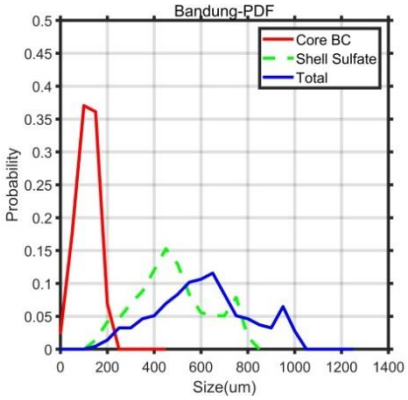

(c)

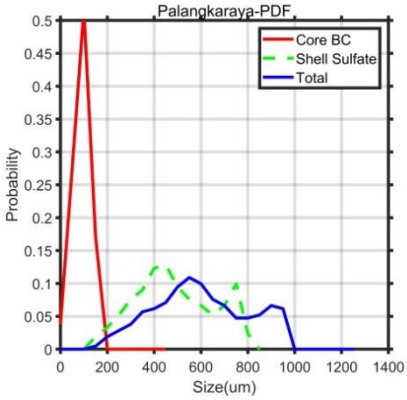

(d)

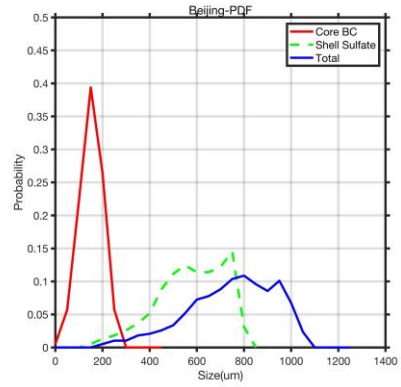

(e)

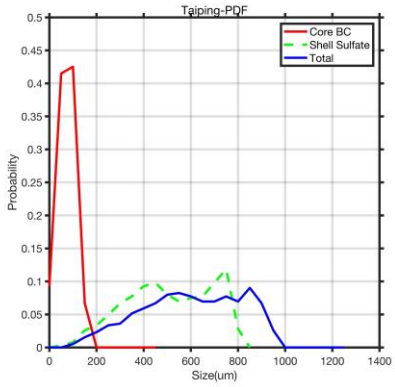

(f)

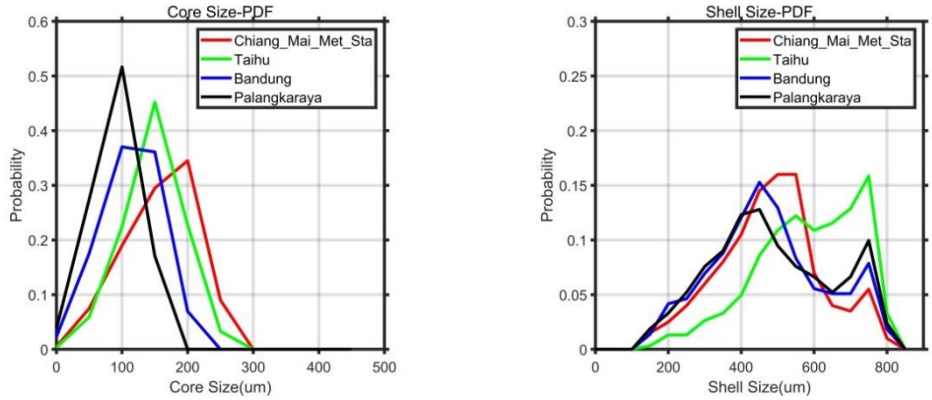

(g) (h)

Figure 3. PDF of the total aerosol particle size, core and shell distribution. (a) Chiang Mai; (b) Taihu; (c) Bandung; (d) Palangkaraya; (e)Beijing; (f) Taiping; (g) core BC size; (h) shell sulfate/nitrogen size.

3.3 Special Cases – Impactful Urban and Long-range Transport

Some sites have different set of characteristics during a subset of the total time series from the overall set of characteristics, allowing multiple categorizations as a function of the times of the year. In particular, some sites generally classified as urban or clean also have a significant but small fraction of their total days that behave either like biomass burning or long-range transport. The two most obvious such cases are Beijing and Taiping island.

The Beijing site is geographically located in an urban area; however, the classification is frequently found to have a biomass burning characteristic. In specific the mean value of AOD in Beijing is higher than Chiang Mai, and the 50^{th} percentile of the STD of AOD is slightly lower than in Chiang Mai. This shows that Beijing has a higher average AOD than in Chiang Mai and less overall variation, consistent with its being an urban site. Similarly, the results of the MIE model show that Beijing generally matches well with Taihu (Figure 2e). However, the larger amount of variability of AOD, wider SSA range leading to lower SSA values than observed at Taihu, all consistent with the wider size of BC core and shell, and in specific possessing a set of larger core sizes and smaller shell sizes than Taihu, yet consistent with the range formed due to a linear combination of urban and biomass burning characteristics. In particular, the solution space of the particle is found to be the widest of all of the sites in

this paper with a 61.3 nm core size range and 154.4 nm shell size range. More similar to the urban characteristic, at smaller particle sizes the SSA of is found to gradually increase, with the median and maximum of the solution space respectively 0.91 and 0.95. The ASR of Beijing is also found to have a wide range, with a median of 3.5, and a range from 2.5 to 4.8. The corresponding AMR is also broad with a range from 6.4 to 59. The result of the probability density function of Beijing shows in Figure 3e. For BC core, the proportion of core larger than 200nm is 68%, while the shell has 38% of measurements between 400nm and 600nm and 50% between 600nm and 800nm.

Taiping island is classified as clean, which is consistent with its location in South China Sea more than 100km from other land. However, if analyzing the data from February and March separately, a new classification of long-range transport is determined. The results of the MIE model show that while the overall characteristics of the solution space of aerosol properties at Taiping island is similar to Palangkaraya (Figure 2f), overall, the particle size is wider than both Palangkaraya and Bandung (55.4 nm core size, 204.2 nm shell size). Furthermore, the total absorption has the highest value of all of the sites analyzed (SSA>0.93). In specific at smaller particle sizes, the SSA of the net aerosol particles is found to gradually increase, although the median and maximum are found to respectively be 0.96 and 0.99. The corresponding ASR and AMR at Taiping island both have a wide range, with a median of 4.6, and a range from 3.38 to 6 for the ASR and a range from 16.4 to 555 for the AMR, consistent with the range of particle sizes spanning both clean and long-range transport types. The result of the probability density function at Taiping island (Figure 3f) show clearly that the BC core sizes are relatively small (the proportion of core larger than 200nm is 0%) and a very thick shell (with 34% between 400nm and 600nm and 37% between 600nm and 800nm) respectively. These results are consistent with the air flow from Eastern India and Northern Southeast Asia containing large amounts of fires which are then strongly advected in the middle troposphere to the east annually during February and March.

Conclusions

This work as demonstrated an objective, clear, and simple way to systematically analyze the regional characteristics of aerosol size and mixing state based on measurements from AERONET sites located throughout East Asia, Southeast

Asia and South Asia. In specific, use of multi-wavelength measurements of AOD, SSA and AE, as well as the standard deviation of AOD and the ratio of the standard deviation of AOD to AOD reveal that aerosols in Asia have at least 4 different fundamental characteristics, corresponding respectively to: urban, biomass burning, long-range transport, and clean.

Applying a Core-Shell based MIE model and constraining the results with the multi-spectral measurements, allows for a solution set of core and shell sizes to be obtained for each AERONET site. It is then revealed that both the core and shell sizes, as well as other aerosol properties including the mixing state and SSA are consistent within each of the 4 categories of aerosol types, and are not otherwise mixed between the different categories of types, showing that these classifications are robust, with the largest BC core sizes being found as expected in biomass burning regions (the AMR ranges from 4.5 to 35 in Chiang Mai), and the thickest shell sizes being found for long-range transport (the AMR in Palangkaraya ranges from 15.3 to 120).

Additionally, two locations were found which had characteristics of different sites, but only when successfully separated based on the time of the year. Heavily urban Beijing is found to be consistent with both urban and biomass burning properties (the overall size range is far wider than in Taihu, with 61.3nm core size range and 154.4 nm shell size range). Very remote Taiping island is found to have both clean and long-range transport characteristics. (AMR ranges from 16.4 to 555). These results confirm that considerable new information can be gleaned from existing AERONET measurements, as well as more evidence for the effects of changes in the attribution of biomass burning, urbanization, and long range transport of sources, all of which are known to be rapidly changing and not well characterized throughout Asia.

Acknowledgments, Samples, and Data

- **General**: We would like to acknowledge the PIs of the AERONET instruments for providing the remote sensing measurements be downloaded from https://aeronet.gsfc.nasa.gov/cgi-bin/draw_map_display_inv_v3.
- **Funding:** The work was supported by the Chinese National Young Thousand Talents Program (Project 41180002), the Chinese National Natural Science

Foundation (Project 41030028; Project 42075147), and the Guangdong Provincial Young Talent Support Fund (Project 42150003).

- **Author contributions:** S. W. processed and analyzed the samples, drafting, modeling; C. J. B. led the project and designed the study and coordinated the discussion; X. W. participated code process and the visualization of the results.
- **Competing interests:** The authors declare no competing interests.
- **Data and materials availability:** All processed data and codes are freely available for download at https://doi.org/10.6084/m9.figshare.14077169

References

Andreae, M., and A. Gelencsér (2006), Black carbon or brown carbon? The nature of light-absorbing carbonaceous aerosols, *Atmospheric Chemistry and Physics*, *6*(10), 3131-3148.

Barsanti, K., A. G. Carlton, and S. H. Chung (2013), Analyzing experimental data and model parameters: implications for predictions of SOA using chemical transport models, *Atmospheric Chemistry and Physics*, *13*(23), 12073-12088.

Bondy, A. L., D. Bonanno, R. C. Moffet, B. Wang, A. Laskin, and A. P. Ault (2018), The diverse chemical mixing state of aerosol particles in the southeastern United States, *Atmospheric chemistry and physics*, *18*(16), 12595-12612.

Cai, M., B. Liang, Q. Sun, S. Zhou, X. Chen, B. Yuan, M. Shao, H. Tan, and J. Zhao (2020), Effects of continental emissions on cloud condensation nuclei (CCN) activity in the northern South China Sea during summertime 2018, *Atmospheric Chemistry and Physics*, *20*(15), 9153-9167.

Charlson, R. J., and T. M. Wigley (1994), Sulfate aerosol and climatic change, *Scientific American*, *270*(2), 48-57.

Chew, B. N., J. R. Campbell, S. V. Salinas, C. W. Chang, J. S. Reid, E. J. Welton, B. N. Holben, and S. C. Liew (2013), Aerosol particle vertical distributions and optical properties over Singapore, *Atmospheric environment*, *79*, 599-613.

Chung, S. H., and J. H. Seinfeld (2005), Climate response of direct radiative forcing of anthropogenic black carbon, *Journal of Geophysical Research: Atmospheres*, *110*(D11).

Cohen, J. B. (2014), Quantifying the occurrence and magnitude of the Southeast Asian fire climatology, *Environmental Research Letters*, *9*(11), 114018.

Cohen, J. B., and R. G. Prinn (2011), Development of a fast, urban chemistry metamodel for inclusion in global models, *Atmospheric Chemistry and Physics*, *11*(15), 7629-7656.

Cohen, J. B., and C. Wang (2014), Estimating global black carbon emissions using a top-down Kalman Filter approach, *Journal of Geophysical Research: Atmospheres*, *119*(1), 307-323.

Cohen, J. B., R. G. Prinn, and C. Wang (2011), The impact of detailed urban-scale processing on the composition, distribution, and radiative forcing of anthropogenic aerosols, *Geophysical research letters*, *38*(10).

Cohen, J. B., E. Lecoeur, and D. Hui Loong Ng (2017), Decadal-scale relationship between measurements of aerosols, land-use change, and fire over Southeast Asia, *Atmospheric Chemistry and Physics*, *17*(1), 721-743.

Deng, W., J. B. Cohen, S. Wang, and C. Lin (2020), Improving the understanding between climate variability and observed extremes of global NO2 over the past 15 years, *Environmental Research Letters*.

Dubovik, O., A. Smirnov, B. Holben, M. King, Y. Kaufman, T. Eck, and I. Slutsker (2000), Accuracy assessments of aerosol optical properties retrieved from Aerosol Robotic Network (AERONET) Sun and sky radiance measurements, *Journal of Geophysical Research: Atmospheres*, *105*(D8), 9791-9806.

Dubovik, O., B. Holben, T. F. Eck, A. Smirnov, Y. J. Kaufman, M. D. King, D. Tanré, and I. Slutsker (2002), Variability of absorption and optical properties of key aerosol types observed in worldwide locations, *Journal of the atmospheric sciences*, *59*(3), 590-608.

Fast, J. D., W. I. Gustafson Jr, R. C. Easter, R. A. Zaveri, J. C. Barnard, E. G. Chapman, G. A. Grell, and S. E. Peckham (2006), Evolution of ozone, particulates, and aerosol direct radiative forcing in the vicinity of Houston using a fully coupled meteorology-chemistry-aerosol model, *Journal of Geophysical Research: Atmospheres*, *111*(D21).

Haywood, J., and K. Shine (1995), The effect of anthropogenic sulfate and soot aerosol on the clear sky planetary radiation budget, *Geophysical Research Letters*, *22*(5), 603-606.

Holben, B. N., T. F. Eck, I. a. Slutsker, D. Tanre, J. Buis, A. Setzer, E. Vermote, J. A. Reagan, Y. Kaufman, and T. Nakajima (1998), AERONET—A federated instrument network and data archive for aerosol characterization, *Remote sensing of environment*, *66*(1), 1-16.

Ichoku, C., and L. Ellison (2014), Global top-down smoke-aerosol emissions estimation using satellite fire radiative power measurements, *Atmospheric Chemistry and Physics*, *14*(13), 6643-6667.

Ichoku, C., L. Giglio, M. J. Wooster, and L. A. Remer (2008), Global characterization of biomass-burning patterns using satellite measurements of fire radiative energy, *Remote Sensing of Environment*, *112*(6), 2950-2962.

Jacobson, M. Z. (2001), Strong radiative heating due to the mixing state of black carbon in atmospheric aerosols, *Nature*, *409*(6821), 695-697.

Kahn, R., P. Banerjee, D. McDonald, and D. J. Diner (1998), Sensitivity of multiangle imaging to aerosol optical depth and to pure-particle size distribution and composition over ocean, *Journal of Geophysical Research: Atmospheres*, *103*(D24), 32195-32213.

Kahn, R. A., B. J. Gaitley, M. J. Garay, D. J. Diner, T. F. Eck, A. Smirnov, and B. N. Holben (2010), Multiangle Imaging SpectroRadiometer global aerosol product assessment by comparison with the Aerosol Robotic Network, *Journal of Geophysical Research: Atmospheres*, *115*(D23).

Kahnert, M., T. Nousiainen, and H. Lindqvist (2013), Models for integrated and differential scattering optical properties of encapsulated light absorbing carbon aggregates, *Optics express*, *21*(7), 7974-7993.

Kajino, M., Y. Inomata, K. Sato, H. Ueda, Z. Han, J. An, G. Katata, M. Deushi, T. Maki, and N. Oshima (2012), Development of the RAQM2 aerosol chemical transport model and predictions of the Northeast Asian aerosol mass, size, chemistry, and mixing type, *Atmospheric Chemistry and Physics*, *12*(24), 11833-11856.

Kim, D., C. Wang, A. M. Ekman, M. C. Barth, and P. J. Rasch (2008), Distribution and direct radiative forcing of carbonaceous and sulfate aerosols in an interactive size-resolving aerosol–climate model, *Journal of geophysical research: Atmospheres*, *113*(D16).

Kim, P. S., D. J. Jacob, J. A. Fisher, K. Travis, K. Yu, L. Zhu, R. M. Yantosca, M. Sulprizio, J. L. Jimenez, and P. Campuzano-Jost (2015), Sources, seasonality, and trends of southeast US aerosol: an integrated analysis of surface, aircraft, and satellite observations with the GEOS-Chem chemical transport model, *Atmospheric Chemistry and Physics*, *15*(18), 10411-10433.

Lane, T. E., N. M. Donahue, and S. N. Pandis (2008), Simulating secondary organic aerosol formation using the volatility basis-set approach in a chemical transport model, *Atmospheric Environment*, *42*(32), 7439-7451.

Langmann, B., B. Duncan, C. Textor, J. Trentmann, and G. R. Van Der Werf (2009), Vegetation fire emissions and their impact on air pollution and climate, *Atmospheric environment*, *43*(1), 107-116.

Lin, C., J. B. Cohen, S. Wang, and R. Lan (2020a), Application of a combined standard deviation and mean based approach to MOPITT CO column data, and resulting improved representation of biomass burning and urban air pollution sources, *Remote Sensing of Environment*, *241*, 111720.

Lin, C., J. B. Cohen, S. Wang, R. Lan, and W. Deng (2020b), A new perspective on the spatial, temporal, and vertical distribution of biomass burning: quantifying a significant increase in CO emissions, *Environmental Research Letters*, *15*(10), 104091.

Lin, C.-Y., C. Zhao, X. Liu, N.-H. Lin, and W.-N. Chen (2014), Modelling of long-range transport of Southeast Asia biomass-burning aerosols to Taiwan and their radiative forcings over East Asia, *Tellus B: Chemical and Physical Meteorology*, *66*(1), 23733.

Matsui, H., M. Koike, Y. Kondo, N. Moteki, J. D. Fast, and R. A. Zaveri (2013), Development and validation of a black carbon mixing state resolved three-dimensional model: Aging processes and radiative impact, *Journal of Geophysical Research: Atmospheres*, *118*(5), 2304-2326.

Ming, Y., V. Ramaswamy, and G. Persad (2010), Two opposing effects of absorbing aerosols on global-mean precipitation, *Geophysical Research Letters*, *37*(13).

Nordmann, S., Y. Cheng, G. Carmichael, M. Yu, H. Denier Van Der Gon, Q. Zhang, P. Saide, U. Pöschl, H. Su, and W. Birmili (2014), Atmospheric black carbon and warming effects influenced by the source and absorption enhancement in central Europe, *Atmospheric Chemistry and Physics*, *14*(23), 12683-12699.

Parry, M., M. L. Parry, O. Canziani, J. Palutikof, P. Van der Linden, and C. Hanson (2007), *Climate change 2007-impacts, adaptation and vulnerability: Working group II contribution to the fourth assessment report of the IPCC*, Cambridge University Press.

Peng, J., M. Hu, S. Guo, Z. Du, J. Zheng, D. Shang, M. L. Zamora, L. Zeng, M. Shao, and Y.-S. Wu (2016), Markedly enhanced absorption and direct radiative forcing of black carbon under polluted urban environments, *Proceedings of the National Academy of Sciences*, *113*(16), 4266-4271.

574 Ramanathan, V., and G. Carmichael (2008), Global and regional climate changes due
575 to black carbon, *Nature geoscience*, *1*(4), 221-227.
576 Reuter, M., M. Buchwitz, A. Hilboll, A. Richter, O. Schneising, M. Hilker, J.
577 Heymann, H. Bovensmann, and J. Burrows (2014), Decreasing emissions of NO x
578 relative to CO 2 in East Asia inferred from satellite observations, *Nature Geoscience*,
579 *7*(11), 792-795.
580 Rosenfeld, D. (1999), TRMM observed first direct evidence of smoke from forest
581 fires inhibiting rainfall, *Geophysical research letters*, *26*(20), 3105-3108.
582 Rosenfeld, D., M. O. Andreae, A. Asmi, M. Chin, G. de Leeuw, D. P. Donovan, R.
583 Kahn, S. Kinne, N. Kivekäs, and M. Kulmala (2014), Global observations of aerosol-
584 cloud-precipitation-climate interactions, *Reviews of Geophysics*, *52*(4), 750-808.
585 Schuster, G. L., O. Dubovik, B. N. Holben, and E. E. Clothiaux (2005), Inferring
586 black carbon content and specific absorption from Aerosol Robotic Network
587 (AERONET) aerosol retrievals, *Journal of Geophysical Research: Atmospheres*,
588 *110*(D10).
589 Schutgens, N. A. J., and P. Stier (2014), A pathway analysis of global aerosol
590 processes, *Atmos. Chem. Phys.*, *14*(21), 11657-11686.
591 Sinyuk, A., O. Dubovik, B. Holben, T. F. Eck, F.-M. Breon, J. Martonchik, R. Kahn,
592 D. J. Diner, E. F. Vermote, and J.-C. Roger (2007), Simultaneous retrieval of aerosol
593 and surface properties from a combination of AERONET and satellite data, *Remote*
594 *Sensing of Environment*, *107*(1-2), 90-108.
595 Stockwell, W. R., P. Middleton, J. S. Chang, and X. Tang (1990), The second
596 generation regional acid deposition model chemical mechanism for regional air
597 quality modeling, *Journal of Geophysical Research: Atmospheres*, *95*(D10),
598 16343-16367.
599 Tang, W., D. Cohan, L. Lamsal, X. Xiao, and W. Zhou (2013), Inverse modeling of
600 Texas NO x emissions using space-based and ground-based NO 2 observations,
601 *Atmospheric Chemistry and Physics*, *13*(21), 11005-11018.
602 Tao, W. K., J. P. Chen, Z. Li, C. Wang, and C. Zhang (2012), Impact of aerosols on
603 convective clouds and precipitation, *Reviews of Geophysics*, *50*(2).
604 Van Donkelaar, A., R. V. Martin, M. Brauer, N. C. Hsu, R. A. Kahn, R. C. Levy, A.
605 Lyapustin, A. M. Sayer, and D. M. Winker (2016), Global estimates of fine
606 particulate matter using a combined geophysical-statistical method with information

607 from satellites, models, and monitors, *Environmental science & technology*, *50*(7),
608 3762-3772.
609 Wang, C. (2013), Impact of anthropogenic absorbing aerosols on clouds and
610 precipitation: A review of recent progresses, *Atmospheric research*, *122*, 237-249.
611 Wang, S., J. B. Cohen, C. Lin, and W. Deng (2020a), Constraining the relationships
612 between aerosol height, aerosol optical depth and total column trace gas
613 measurements using remote sensing and models, *Atmospheric Chemistry and Physics*,
614 *20*(23), 15401-15426.
615 Wang, S., J. B. Cohen, W. Deng, K. Qin, and J. Guo (2020b), Using a New
616 Top-Down Constrained Emissions Inventory to Attribute the Previously Unknown
617 Source of Extreme Aerosol Loadings Observed Annually in the Monsoon Asian Free
618 Troposphere, *Earth and Space Science Open Archive*, 27, 2020,
619 doi:10.1002/essoar.10505441.1
620 Weagle, C. L., G. Snider, C. Li, A. van Donkelaar, S. Philip, P. Bissonnette, J. Burke,
621 J. Jackson, R. Latimer, and E. Stone (2018), Global sources of fine particulate matter:
622 interpretation of PM2. 5 chemical composition observed by SPARTAN using a global
623 chemical transport model, *Environmental science & technology*, *52*(20),
624 11670-11681.
625 Yu, F., G. Luo, and X. Ma (2012), Regional and global modeling of aerosol optical
626 properties with a size, composition, and mixing state resolved particle microphysics
627 model, *Atmospheric Chemistry and Physics*, *12*(13), 5719-5736.
628 Yuan, J.-F., X.-F. Huang, L.-M. Cao, J. Cui, Q. Zhu, C.-N. Huang, Z.-J. Lan, and
629 L.-Y. He (2016), Light absorption of brown carbon aerosol in the PRD region of
630 China, *Atmospheric Chemistry and Physics*, *16*(3), 1433-1443.
631 Zaveri, R. A., R. C. Easter, J. D. Fast, and L. K. Peters (2008), Model for simulating
632 aerosol interactions and chemistry (MOSAIC), *Journal of Geophysical Research:*
633 *Atmospheres*, *113*(D13).
634 Zhang, R., J. Peng, Y. Wang, and M. Hu (2016), Reply to Boucher et al.: Rate and
635 timescale of black carbon aging regulate direct radiative forcing, *Proceedings of the*
636 *National Academy of Sciences*, *113*(35), E5094-E5095.
637 Zhang, R., A. F. Khalizov, J. Pagels, D. Zhang, H. Xue, and P. H. McMurry (2008),
638 Variability in morphology, hygroscopicity, and optical properties of soot aerosols

during atmospheric processing, *Proceedings of the National Academy of Sciences*, *105*(30), 10291-10296.

Zhang, R., I. Suh, J. Zhao, D. Zhang, E. C. Fortner, X. Tie, L. T. Molina, and M. J. Molina (2004), Atmospheric new particle formation enhanced by organic acids, *Science*, *304*(5676), 1487-1490.